Inorganic Chemistry

pubs.acs.org/IC Article

Quasi-One-Dimensional Transition-Metal Chalcogenide Semiconductor $(Nb_4Se_{15}I_2)I_2$

Kejian Qu, Zachary W. Riedel, Irián Sánchez-Ramírez, Simon Bettler, Junseok Oh, Emily N. Waite, Toby J. Woods, Nadya Mason, Peter Abbamonte, Fernando de Juan, Maia G. Vergniory, and Daniel P. Shoemaker*

Cite This: *Inorg. Chem.* 2023, 62, 3067−3074 Read Online

ACCESS | Metrics & More | Article Recommendations | Supporting Information

ABSTRACT: The discovery of new low-dimensional transition-metal chalcogenides is contributing to the already prosperous family of these materials. In this study, needle-shaped single crystals of a quasi-one-dimensional (1D) material, $(Nb_4Se_{15}I_2)I_2$, were grown by chemical vapor transport, and the structure was solved by single-crystal X-ray diffraction (XRD). The structure has 1D $(Nb_4Se_{15}I_2)_n$ chains along the [101] direction, with two I^- ions per formula unit directly bonded to Nb^{5+}. The other two I^- ions are loosely coordinated and intercalated between the chains. Individual chains are chiral and stack along the *b* axis in opposing directions, giving space group $P2_1/c$. The phase purity and crystal structure were verified by powder XRD. Density functional theory calculations show $(Nb_4Se_{15}I_2)I_2$ to be a semiconductor with a direct band gap of around 0.6 eV. Resistivity measurements of bulk crystals and micropatterned devices demonstrate that $(Nb_4Se_{15}I_2)I_2$ has an activation energy of around 0.1 eV, and no anomaly or transition was seen upon cooling. Low-temperature XRD shows that $(Nb_4Se_{15}I_2)I_2$ does not undergo a structural phase transformation from room temperature to 8.2 K, unlike related compounds $(NbSe_4)_nI$ (n = 2, 3, or 3.33), which all exhibit charge-density waves. This compound represents a well-characterized and valence-precise member of a diverse family of anisotropic transition-metal chalcogenides.

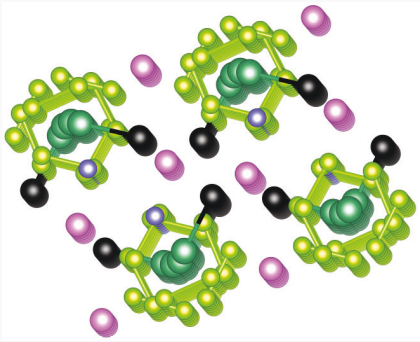

INTRODUCTION

Low-dimensional transition-metal chalcogenides have been under intensive study for decades, and formative works on their crystal chemistry,[1−3] band structures,[4,5] and structural phase transitions[6] have been conducted since the 1960s. The quasi-one-dimensional (1D) chalcogenides are most recognized for the formation of charge-density waves (CDWs), which exhibit nonlinear transport behavior and gave inspiration to the modulated charge transport in conducting polymers.[7,8] Some of these materials are now undergoing a renaissance because of the possibility of the CDW-induced gapping of electronic bands in Weyl semimetals.[9,10] The propensity for 1D and two-dimensional exfoliation, the strong anisotropy, and their semiconducting behavior with few bands (and thus well-defined orbital contributions to transport) at the Fermi level are among the major merits of transition-metal chalcogenides, which have been reviewed extensively by Manzeli et al.[11] and Petra and Rout.[12] Despite a sustained interest in this class of materials, the precise mechanisms that lead to their synthesis and transport are still under investigation, and accordingly the landscape of stable phases has not been fully explored.

CDW formation is one of the defining hallmark properties of some transition-metal chalcogenides.[13] When a CDW forms, a uniform electronic band modulates its density and creates a superlattice, which is often incommensurate with the high-temperature structural unit cell. The electronic modulation leads to a corresponding distortion of the atomic structure. In the simplest conceptual model, a Peierls distortion, a metallic material will transform into a semiconductor upon cooling due to electron localization, supercell formation, and the creation of a band gap. Quasi-1D materials such as $NbSe_3$[14,15] and TaS_3[16−18] undergo CDW transitions, where a simple interpretation would predict a Peierls distortion along the 1D chains below their respective CDW transition temperatures. In reality, the band structures are complex, and there are many ways to lower the electronic energies of these systems, so CDW wavevectors are often not along the quasi-1D direction, or they may form in multiple directions. Low-temperature X-ray diffraction (XRD) or electron diffraction is typically the most clear evidence of these CDW transitions and orderings: when superlattices form due to the onset of a CDW, satellite reflections around the main Bragg reflections are apparent in $NbSe_3$ and TaS_3.[15,19] Another key signature of

Received: October 27, 2022
Published: February 9, 2023

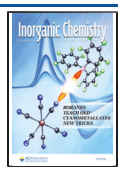

https://doi.org/10.1021/acs.inorgchem.2c03796
Inorg. Chem. 2023, 62, 3067−3074

CDW transitions is the deviation from Arrhenius resistivity behavior, which is embodied by the nonlinearity of the logarithmic resistivity $\ln(\rho)$ versus $1/T$, such as the steep increase in resistivity seen at 240 K for monoclinic TaS_3 and at 145 and 59 K in $NbSe_3$[19,20] as the temperature decreases.

Closely related to $NbSe_3$ and TaS_3, ternary quasi-1D transition-metal chalcogenides have I intercalated between the chains,[21] such as $(TaSe_4)_2I$ (space group $I422$),[22] $(NbSe_4)_2I$ [isostructural with $(TaSe_4)_2I$], $(NbSe_4)_3I$ (space group $P4/mnc$),[23] and $(NbSe_4)_{3.33}I$ (space group $P4/mcc$).[24] These materials have $(TaSe_4)_n$ or $(NbSe_4)_n$ chains along the c axis, with all Se ions dimerized into $(Se_2)^{2-}$ units and bonded to either Ta or Nb. Ta and Nb ions have alternating 4+ and 5+ valences, leaving the $(TaSe_4)_n$ or $(NbSe_4)_n$ chain with partially filled conducting d bands. $(TaSe_4)_2I$,[8] $(NbSe_4)_2I$,[25] $(NbSe_4)_3I$,[26] and $(NbSe_4)_{3.33}I$[27] undergo CDW transitions, and low-temperature XRD and resistivity measurements were used to demonstrate the onset of the CDW.[28,29] Traditionally, single crystals of $(TaSe_4)_2I$ and $(NbSe_4)_3I$ have been successfully synthesized by chemical vapor transport (CVT)[30] where intermediate gaseous species deposit the target compounds at the low-temperature side of the reaction vessel at temperatures ranging from 400 to 800 °C.[21,31] $(TaSe_4)_2I$ is currently under renewed focus, particularly due to claims that it may harbor "axion insulator" behavior if the CDW wavevector is coincident with one of the Ta d bands crossing the Fermi energy, the location of which is termed a Weyl point due to the chirality of the compound.[32,33] The band crossing at the Fermi energy of $(TaSe_4)_2I$ is a clue that the material may host a CDW transition,[34−36] although it turns out that the CDW wavevector in $(TaSe_4)_2I$ is not coincident with the crossing point.[37] Because of the complexities of these materials and the urgent need to compare and benchmark how charge-transport phenomena correlate with band structures,[38] it is of great interest to discover new transition-metal chalcogenides with similar elemental compositions and quasi-1D structure.

Here we present a quasi-1D compound, $(Nb_4Se_{15}I_2)I_2$, with a structure related to $(TaSe_4)_2I$ and $(NbSe_4)_3I$. Formed from analogous CVT reactions, $(Nb_4Se_{15}I_2)I_2$ is a band insulator with a single Se per formula unit acting as a divalent (nondimerized) ion and two of the four I^- ions present in the 1D chain; hence, the formula is deliberately written as $(Nb_4Se_{15}I_2)I_2$, instead of simply $Nb_4Se_{15}I_4$. The complex chain stoichiometry enforces valence-precise Nb^{5+}, and our transport, diffraction, and density functional theory (DFT) examinations conclude that $(Nb_4Se_{15}I_2)I_2$ is a band insulator without a CDW transition because no electronic bands cross the Fermi energy.

METHODS

Synthesis. The CVT synthesis of $(Nb_4Se_{15}I_2)I_2$ gained its insight from the CVT synthesis of $(TaSe_4)_2I$,[31] and the results depend heavily on details, including sample mass, stoichiometry, form (powder or wire) of ingredients, temperature profile, etc. Elements were ground in an agate mortar with a molar ratio of Nb (99.8%, powder):Se (99.999%, ground shots):I (99.8%, crystalline solid) = 2:8:10.3. The excess 0.3 I was intentionally added to compensate for the loss from sublimation, and the ratio of I was larger than any known Nb−Se−I ternary compounds, to ensure that enough I was available to act as the transport agent. The total sample mass was about 0.9 g. After it was fully ground with a pestle, the mixture tended to form a porous, loosely bound agglomerate, and Nb powder did not stick to the surface of the mortar. The powder mixture was loaded into a fused quartz tube, which was sealed under vacuum. The sealed tube was heated in a horizontal two-zone furnace with high- and low-temperature sides at 420 and 280 °C. The furnace was programmed so that both sides reached their temperature set points simultaneously after 10 h and was held for 90 h before cooling naturally.

Dense needle-shaped crystals formed on the inner wall of the tube in a large region where the temperature ranges from roughly 350 to 290 °C. The crystals did not form directly on the wall, but on a layer of I (or I-containing compound), which coated the lower-temperature half of the tube after reaction. A picture of the tubes after reaction is shown in Figure S1.[39] The typical dimensions of these crystals are 5 × 0.1 × 0.1 mm. Some crystals are ribbon-shaped, with a thickness even smaller than 0.1 mm, while the maximum sizes observed were around 10 × 0.5 × 0.5 mm. Loose powders of $(NbSe_4)_3I$ formed as a residue at the high-temperature side of the tube. Slightly different temperature profiles were attempted and $(Nb_4Se_{15}I_2)I_2$ crystals were obtained, but the size and yield of the crystals were inferior to the aforementioned temperature profile and the byproduct $(NbSe_4)_3I$ had a much larger yield. This further indicates the sensitivity of the reaction to the reaction conditions. Similar reactions of direct combinations of elements using a Se shot, without a temperature gradient, produced $(NbSe_4)_2I$ and $(NbSe_4)_3I$ but not $(Nb_4Se_{15}I_2)I_2$.

Structure Determination. Single-crystal XRD was performed on a Bruker D8 Venture Duo diffractometer at room temperature (23.0 °C) with the sample sitting on a loop in oil. The structure of $(Nb_4Se_{15}I_2)I_2$ was solved with *SHELX* using the intrinsic phasing algorithm.[40] The structure was refined with *SHELXL*[41] in *OLEX2*.[42] Seven outlier reflections (error/esd > 10, as determined by *SHELX*) were omitted from the refinements: (−1 2 1), (0 1 1), (1 25 4), (3 26 3), (3 28 4), (1 22 3), and (0 4 0). The experimental density of $(Nb_4Se_{15}I_2)I_2$ was calculated from a refined cell. All atoms refined to full occupancy within a precision of about 1%. Powder XRD was performed on a Bruker D8 Advance diffractometer using crushed crystals. The needle crystals cannot be ground into fine powder, so hundreds of thin needles were crushed and treated as the powder sample. The result was refined by *GSAS-II*[43] to verify the structure of $(Nb_4Se_{15}I_2)I_2$. Scanning electron microscopy was performed in a ThermoFisher Axia ChemiSEM microscope.

Band-Structure Calculation. First-principles DFT calculations were performed using the Vienna ab initio simulation package (*VASP*)[44,45] with projector-augmented-wave pseudopotentials and two approximations: the Perdew−Burke−Ernzerhof (PBE) parametrization[46] and the modified Becke−Johnson (mBJ) method.[47] The mBJ method was chosen in order to obtain a more accurate description for the band gap of $(Nb_4Se_{15}I_2)I_2$ and to check the validity of the PBE approximation for density of states (DOS) calculations. The electronic band structure was obtained by employing experimental structural data refined by single-crystal XRD, using a plane-wave basis with a kinetic cutoff of 520 eV and a 7 × 3 × 7 k mesh for both approximations. Orbital-resolved DOS results were obtained with a 11 × 5 × 11 k mesh using the tetrahedron method with Blöhl corrections[48] and the PBE approximation. All calculations were performed considering spin−orbit coupling.

Resistivity Measurements. An in-line four-point resistivity measurement was carried out with a Quantum Design Physical Property Measurement System (PPMS). A long, thick, and clean single crystal was chosen, and the contacts were made using Au wires and Ag epoxy. The crystal was approximately 0.5 mm wide and 0.5 mm thick, with two inner voltage leads having a distance of about 1 mm.

As a comparison, one of the crystals was also exfoliated using scotch tape into flakes with thicknesses of less than 100 nm. Electron-beam lithography was used to pattern the electrical contacts into a four-point configuration on these devices, followed by the deposition of Ti(5 nm)/Au(60 nm). A micrograph of the device is shown in Figure S4.[39] The electronic resistance of the device was measured in the PPMS and a custom setup including a Keithley 2400 multimeter.

Phase-Transition Determination. Three-dimensional X-ray maps of momentum space were obtained using a Mo Kα (λ = 0.7107 Å) microspot X-ray source and a Mar345 image-plate detector

https://doi.org/10.1021/acs.inorgchem.2c03796
Inorg. Chem. 2023, 62, 3067−3074

by sweeping crystals through an angular range of 20° with an exposure time of 180 s/image. The sample was first cooled to a base temperature and then warmed up. Diffraction patterns were collected at 8.2, 100, 200, 250, and 290 K. Figures S5 and S6 show the diffraction patterns at 290 and 8.2 K, respectively, with Bragg peaks indexed for 8.2 K.[39]

Differential scanning calorimetry (DSC) was performed using a TA Discovery 2500 calorimeter, cycling in a temperature range of −125 to +25 °C, to rule out any potential phase transitions. The result is shown in Figure S7.[39]

RESULTS AND DISCUSSION

Crystal Structure of $(Nb_4Se_{15}I_2)I_2$. Bundles of needle-shaped single crystals of $(Nb_4Se_{15}I_2)I_2$ grew from common nucleation centers, as shown in Figure 1a. These multi-

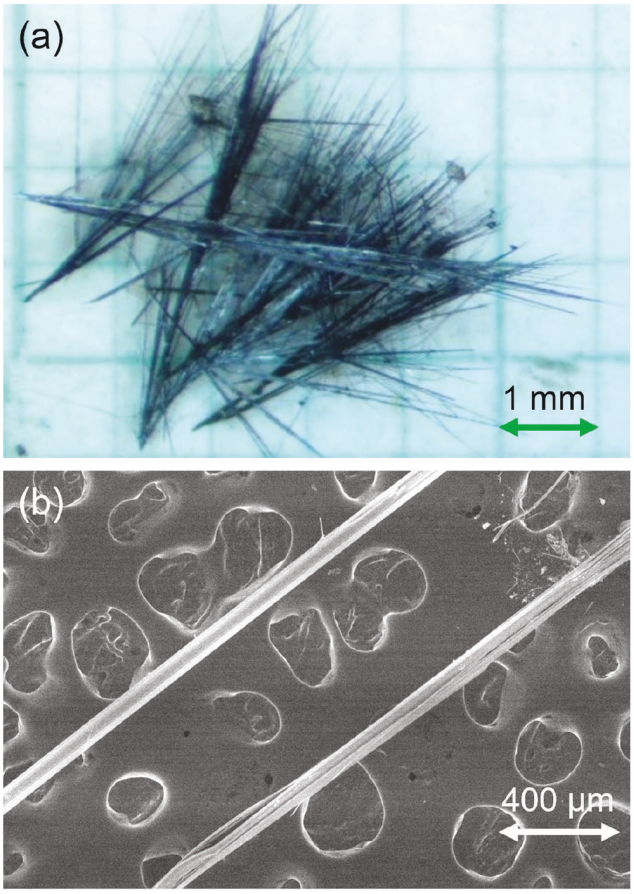

Figure 1. (a) Photograph of typical $(Nb_4Se_{15}I_2)I_2$ crystals obtained from CVT. (b) SEM image of two $(Nb_4Se_{15}I_2)I_2$ crystal bundles on carbon tape.

millimeter single crystals can be easily further exfoliated into thinner strands. Figure 1b shows a SEM micrograph of two exfoliated, thinner needle crystals. The splitting of the strands is more clear in the lower crystal, suggesting weak van der Waals bonding between the chains.

The crystal structure of $(Nb_4Se_{15}I_2)I_2$ was solved from single-crystal XRD, with details shown in Table 1 and atomic positions in Table S1. The unit cell is shown in Figure 2a, where $(Nb_4Se_{15}I_2)_n$ forms 1D chains along the [101] direction (Figure 2b). Half of the I ions (black, intrachain) are directly bonded to Nb ions, while the other half of the I ions (pink, interchain) lie between the chains and are weakly associated,

Table 1. Overview of the Single-Crystal XRD Refinement of $(Nb_4Se_{15}I_2)I_2$[a]

space group	$P2_1/c$
a (Å)	8.8807(2)
b (Å)	25.8368(7)
c (Å)	11.6222(3)
β (deg)	103.437(1)
V (Å^3)	2593.70(11)
Z	4
abs coeff	27.527
exptl density (g/cm^3)	5.285
$F(000)$	3544
no. of reflns	7925
goodness of fit	1.022
no. of param	208
R_{int} (%)	6.08
R_1 (%)	2.36
wR_2 (%)	5.36
I/σ	40.3
d_{min} (Å)	0.70

[a]The atomic positions are given in Table S1.

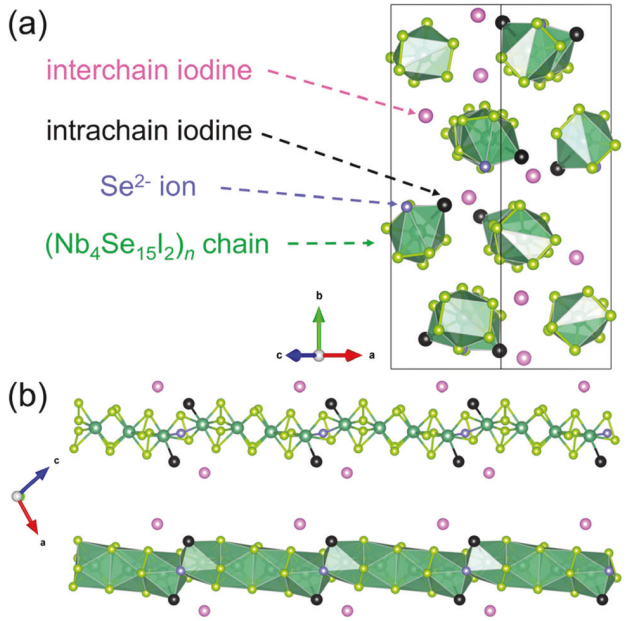

Figure 2. (a) Unit cell of $(Nb_4Se_{15}I_2)I_2$ viewed down the 1D chains showing the hexagonal packing of chains with interchain I^- (pink), intrachain I^- (black), Se^{2-} (light blue), and the majority of Se dimerized as $(Se_2)^{2-}$ (light green). (b) View along b, normal to the 1D chains, highlighting the ions and coordinations with the same color scheme. Two views of an identical chain are shown in part (b): the upper chain shows ions and bonds for clarity, while the lower chain has Nb-centered polyhedra drawn to emphasize the zigzag fashion of the same chain.

with the closest ion being Se at 3.1720(8) Å. This explains why the chemical formula is intentionally written as $(Nb_4Se_{15}I_2)I_2$, in analogy to $(TaSe_4)_2I$, to emphasize the fact that the I ions are split evenly into intra- and interchain positions.

The distance between a Nb ion with the I directly bonded is either 2.8889(7) or 2.9155(7) Å in $(Nb_4Se_{15}I_2)I_2$. On the contrary, the distance between a Nb ion with the closest interchain I has values of 4.5732(7), 4.6011(8), 4.7254(7), and 4.7703(7) Å, depending on which of the four types of Nb ions

https://doi.org/10.1021/acs.inorgchem.2c03796
Inorg. Chem. 2023, 62, 3067−3074

are considered because they have slightly different chemical environments. As a comparison, the Nb−I bonding distances for other Nb−Se−I ternary compounds are similar. For compounds with Nb-bonded I, the distances are 2.994(4) Å for $Nb_4Se_4I_4$[49] and range from 2.7459(10) to 2.9428(9) Å for $Nb_2Se_2I_6$.[50] In these two compounds, all I ions are directly bonded to Nb. On the contrary, the closest Nb−I distance is 4.839(2) Å for $(NbSe_4)_3I$,[23] and 4.8273(5) Å for $(NbSe_4)_{3.33}I$,[24] where all the I ions are interchain. The Nb−I distances for all of these compounds are plotted in Figure 3 to emphasize that half of the I ions in $(Nb_4Se_{15}I_2)I_2$ follow the expected trends for direct intrachain bonding, while the other half are weakly associated interchain ions.

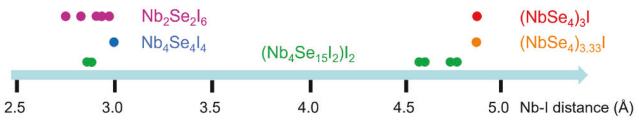

Figure 3. Nb−I distances of Nb−Se−I compounds, demonstrating the difference of intrachain Nb−I bonding (short) and interchain (long) Nb−I distances. Each material may have multiple Nb−I distances.

In each formula unit, 14 Se ions are dimerized and the Se−Se bond distances range from 2.3278(8) to 2.4212(8) Å. Each of these dimerized Se has a 1− valence, while the singular Se ion has a 2− valence. Each Nb ion has a coordination number of 8. Half of the Nb ions bond to four Se−Se pairs, with two pairs forming a rectangular face on each side of the chain direction, while the other half bond to three Se−Se pairs, one Se^{2-}, and an intrachain I^-. The Nb-centered polyhedra are connected by sharing Se-coordinated faces (rectangles for pairs of dimers, triangles for a dimer, and a lone Se^{2-}). I ions only coordinate a single Nb, which leads to jogs in the chain at each I^- position, while the chirality is imposed by the $NbSe_4$ units in the same manner as that in $(NbSe_4)_nI$ phases. These jogs enable the insertion of Se^{2-} and I^- into the chains, which are necessary to fully oxidize Nb^{5+} in the presence of excess I in CVT and because of the inability to accommodate an "extra" interchain I that would oxidize $(NbSe_4)_2I$ ($Nb^{4.5+}$) to a hypothetical $(NbSe_4)_2I_2$ (perfect Nb^{5+}) phase. The valence of all Nb ions is 5+, which suggests that $(Nb_4Se_{15}I_2)I_2$ should be a band insulator because there are no free d electrons, unlike $(NbSe_4)_nI$ or $(TaSe_4)_2I$. $(Nb_4Se_{15}I_2)I_2$ has a space group of $P2_1/c$ (No. 14), with a much lower symmetry than $(TaSe_4)_2I$ [space group $I422$ (No. 97)] because of the divalent Se and two types of I ions. However, one commonality between $(Nb_4Se_{15}I_2)I_2$ and $(TaSe_4)_2I$ is that they both have chiral chains. In $(Nb_4Se_{15}I_2)I_2$, each layer of chains stacked along the [010] direction shares the same chirality, with the screw direction opposed on each successive (010) layer, leading to a material that has no net chirality, as confirmed by the c glide in space group $P2_1/c$.

Powder XRD was carried out to verify the refined crystal structure and the phase purity of the crystals. The Rietveld refined result is shown in Figure 4. Most peaks are weak due to the difficulty of grinding the crystals (see Methods) and the existence of heavy elements and thus high X-ray absorption. All of the peaks matched the calculated positions, and no additional phases were detected by SEM.

Band-Structure Calculations. The band structure of $(Nb_4Se_{15}I_2)I_2$ calculated by DFT-PBE is shown in Figure 5,

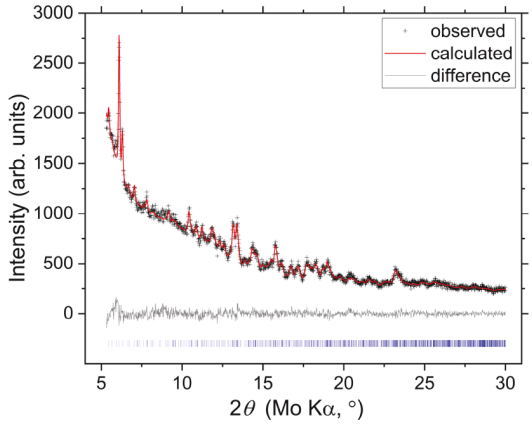

Figure 4. Rietveld refinement to the powder XRD pattern of $(Nb_4Se_{15}I_2)I_2$.

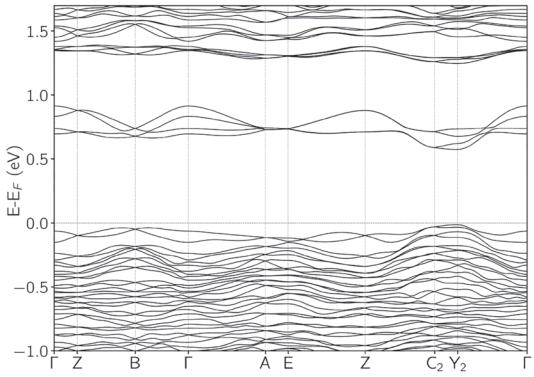

Figure 5. DFT-PBE-calculated electronic band structure of $(Nb_4Se_{15}I_2)I_2$, showing band insulator behavior. The direct band gap at Y_2 is 0.59 eV.

while the DFT-mBJ result is included in Figure S2 as a comparison with PBE.[39] DFT calculations with both approximations predict $(Nb_4Se_{15}I_2)I_2$ to be a semiconductor with a direct band gap. For the PBE approximation, the band gap is direct at Y_2 and E_g = 0.59 eV, while the mBJ-obtained band gap is also direct at Y_2 and E_g = 0.68 eV. Both approximations give very similar results.

The most notable feature of this band structure is an isolated group of eight bands that comprise the conduction band minimum, which combine to form a peak around 0.7 eV in the electronic DOS, as shown in Figure 6. The dispersion of electronic bands along the chain direction (Γ−A) is much larger than that along a direction perpendicular to the chain (A−E), which reflects the existence of linear moieties in $(Nb_4Se_{15}I_2)I_2$. The character of these bands are mainly Nb d and Se p orbitals. To differentiate $(Nb_4Se_{15}I_2)I_2$ from $(TaSe_4)_2I$ and other compounds with mixed valence, we can separate Nb ions into those bonded to I^- (Nb-b) and those unbonded to I^- (Nb-u) and compare their contributions to the DOS in Figure 6b, with a focus just above E_F. Figure S3 shows the DOS contributions from Nb bonded and unbonded I^- in the whole range, and they are essentially identical.[39] The main Nb contribution to the set of eight conduction bands comes from d_{xz} and d_{z^2} orbitals. While strictly linear chains, such as those in $(NbSe_4)_2I$ or $(TaSe_4)_2I$, have orbital occupation near E_F of d_{z^2} only,[51] chains in $(Nb_4Se_{15}I_2)I_2$ have a sideways step every fourth Nb, which necessitates occupation of another

https://doi.org/10.1021/acs.inorgchem.2c03796
Inorg. Chem. 2023, 62, 3067−3074

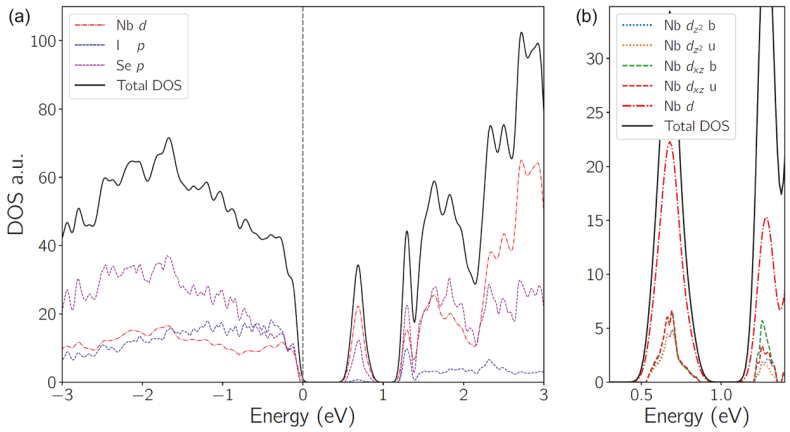

Figure 6. (a) DOS of $(Nb_4Se_{15}I_2)I_2$, projected onto different types of atoms. (b) DOS further projected on Nb d orbitals, separating the I-bonded (Nb-b) and I-unbonded (Nb-u) Nb ions.

orbital. Both sets of Nb [Nb-b bonded to I^- and Nb-u bonded to $(Se_2)^{2-}$ only] are electronically equivalent around the valence band maximum and eight low-energy conduction bands, with some minor differences around 1.2 eV above E_F. This similarity confirms that the charge is not highly modulated along the chain and the assignment of Nb^{5+} is consistent throughout the compound. Without mixed valence on Nb, the Nb 4d orbitals are unoccupied, far from the Fermi energy, and there is no conducting state that would be expected to lead to a CDW.

Phase-Transition Determination. In order to determine if $(Nb_4Se_{15}I_2)I_2$ undergoes a CDW phase transition, like $(TaSe_4)_2I$ does, an in-line four-point resistivity measurement was done on a large bulk needle-shaped $(Nb_4Se_{15}I_2)I_2$ crystal, and the result is shown in Figure 7. The resistivity increases

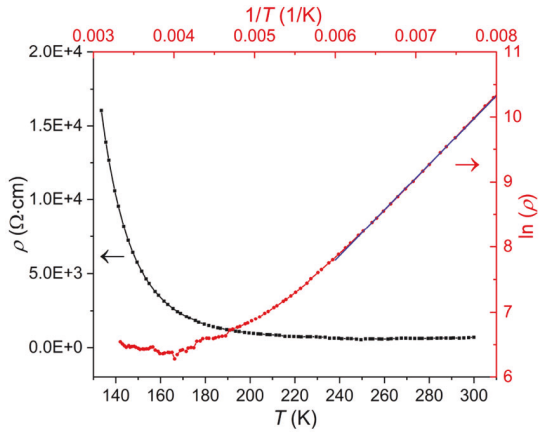

Figure 7. Four-point resistivity of a bulk $(Nb_4Se_{15}I_2)I_2$ crystal. The black and red dots and lines show ρ versus T and $\ln(\rho)$ versus $1/T$, respectively. The blue straight line fits part of the $\ln(\rho)$ versus $1/T$ curve, and the Arrhenius equation was fit to determine the activation energy E_a.

with decreasing temperature until the resistance exceeds the range of measurement. The $\ln(\rho)$ versus $1/T$ curve was also plotted in red in Figure 7, and the empirical Arrhenius fitting $\rho = \rho_0 \exp(E_a/k_BT)$ was done for the linear part of the curve. Here E_a is the activation energy, which can be smaller than half of the band gap E_g, because the material may contain shallow defects that have energies in the band gap. The calculated activation energy is E_a = 0.1 eV, much smaller than the DFT-calculated band gap E_g = 0.6 eV. From resistivity measurements, $(Nb_4Se_{15}I_2)I_2$ behaves like a normal semiconductor upon cooling from 300 to 140 K. No sign of a CDW anomaly has been observed.

As a comparison, a nanodevice was made on an exfoliated $(Nb_4Se_{15}I_2)I_2$ crystal (see Methods), and the result is shown in Figure S4.[39] Only a small portion of the data are shown because the nanodevice became highly resistive at low temperature and the Si substrate contributed to the resistance. The activation energy determined was 0.06 eV, close to that of the bulk crystal.

Room temperature and cryogenic XRD were performed on single-crystal $(Nb_4Se_{15}I_2)I_2$, and the results are shown in Figure S5 (290 K) and Figure S6 (8.2 K).[39] The diffraction pattern did not change as the sample was warmed from 8.2 K to room temperature, nor did satellite peaks form. This demonstrated that there is no structural transformation, whether driven by a CDW or any other instability, between room temperature and 8.2 K.

Finally, DSC was performed on $(Nb_4Se_{15}I_2)I_2$, with the results shown in Figure S7.[39] No transition peaks can be seen in the range of 148−298 K.

The resistivity measurements, low-temperature single-crystal XRD, and DSC measurements did not show evidence of any phase transformations upon cooling $(Nb_4Se_{15}I_2)I_2$. Taking the band structure calculated by DFT into consideration, as well as the fact that all Nb ions are charge-balanced, it can be concluded that, unlike $(TaSe_4)_2I$, $(Nb_4Se_{15}I_2)I_2$ is a semiconductor with a moderate band gap, chiral chains, but no instability or partially filled bands that would lead to a CDW.

CONCLUSIONS

Single crystals of a new transition-metal chalcogenide, $(Nb_4Se_{15}I_2)I_2$, were grown by CVT, and the crystal structure was solved. DFT predicts $(Nb_4Se_{15}I_2)I_2$ to be a semiconductor with a band gap of around 0.6 eV. Resistivity measurements showed the Arrhenius activation energy to be 0.1 eV, likely signifying shallow defect energy levels. Low-temperature XRD and DSC did not show evidence of any phase transformation, and $(Nb_4Se_{15}I_2)I_2$ demonstrated itself to be a band insulator with a moderate band gap. It remains to be seen whether $(Nb_4Se_{15}I_2)I_2$ can have its band structure engineered by chemical doping, applied fields, or external strain. Because of

https://doi.org/10.1021/acs.inorgchem.2c03796
Inorg. Chem. 2023, 62, 3067−3074

the complexities of transport measurements carried out on related materials such as $(TaSe_4)_2I$, it is important to verify how differences in the electronic structure or symmetry might allow or preclude the observed magnetoresistance data that are thought to arise from Weyl or axion behavior. Furthermore, structure types and motifs in this class of materials are still being discovered, which may yet result in more exotic transport phenomena than have yet been proposed.

■ ASSOCIATED CONTENT

Supporting Information

The Supporting Information is available free of charge at https://pubs.acs.org/doi/10.1021/acs.inorgchem.2c03796.

> Image of reaction tubes after CVT, a table with atomic positions of $(Nb_4Se_{15}I_2)I_2$, DFT-PBE and DFT-mBJ band structure calculations, DOS of I-bonded and I-unbonded Nb in the whole DFT range, resistivity measurement of a nanodevice, single-crystal XRD at 290 and 8.2 K with indexing, and DSC result (PDF)

Accession Codes

CCDC 2215551 contains the supplementary crystallographic data for this paper. These data can be obtained free of charge via www.ccdc.cam.ac.uk/data_request/cif, or by emailing data_request@ccdc.cam.ac.uk, or by contacting The Cambridge Crystallographic Data Centre, 12 Union Road, Cambridge CB2 1EZ, UK; fax: +44 1223 336033.

■ AUTHOR INFORMATION

Corresponding Author

Daniel P. Shoemaker − *Department of Materials Science and Engineering and Materials Research Laboratory, University of Illinois at Urbana−Champaign, Urbana, Illinois 61801, United States;* orcid.org/0000-0003-3650-7551; Email: dpshoema@illinois.edu

Authors

Kejian Qu − *Department of Physics and Materials Research Laboratory, University of Illinois at Urbana−Champaign, Urbana, Illinois 61801, United States;* orcid.org/0000-0002-7189-537X

Zachary W. Riedel − *Department of Materials Science and Engineering and Materials Research Laboratory, University of Illinois at Urbana−Champaign, Urbana, Illinois 61801, United States;* orcid.org/0000-0001-5848-5520

Irián Sánchez-Ramírez − *Donostia International Physics Center, Donostia-San Sebastian 20018, Spain*

Simon Bettler − *Department of Physics and Materials Research Laboratory, University of Illinois at Urbana−Champaign, Urbana, Illinois 61801, United States*

Junseok Oh − *Department of Physics and Materials Research Laboratory, University of Illinois at Urbana−Champaign, Urbana, Illinois 61801, United States*

Emily N. Waite − *Department of Physics and Materials Research Laboratory, University of Illinois at Urbana−Champaign, Urbana, Illinois 61801, United States;* orcid.org/0000-0003-2948-5884

Toby J. Woods − *George L. Clark X-Ray Facility and 3M Materials Laboratory, University of Illinois at Urbana−Champaign, Urbana, Illinois 61801, United States;* orcid.org/0000-0002-1737-811X

Nadya Mason − *Department of Physics and Materials Research Laboratory, University of Illinois at Urbana−Champaign, Urbana, Illinois 61801, United States*

Peter Abbamonte − *Department of Physics and Materials Research Laboratory, University of Illinois at Urbana−Champaign, Urbana, Illinois 61801, United States*

Fernando de Juan − *Donostia International Physics Center, Donostia-San Sebastian 20018, Spain; Ikerbasque, Basque Foundation for Science, Bilbao 48013, Spain*

Maia G. Vergniory − *Donostia International Physics Center, Donostia-San Sebastian 20018, Spain; The Max Planck Institute for Chemical Physics of Solids, Dresden 01187, Germany*

Complete contact information is available at: https://pubs.acs.org/10.1021/acs.inorgchem.2c03796

Notes

The authors declare no competing financial interest.

■ ACKNOWLEDGMENTS

Crystal growth, transport, and microstructure characterization were supported by the Center for Quantum Sensing and Quantum Materials, an Energy Frontier Research Center funded by the U.S. Department of Energy, Office of Science, Basic Energy Sciences, under Award DE-SC0021238. The authors acknowledge the use of microscopy facilities at the Materials Research Laboratory Central Research Facilities, University of Illinois, partially supported by National Science Foundation through the University of Illinois Materials Research Science and Engineering Center (Grant DMR-1720633). S.B. acknowledges support through the Early Postdoc Mobility Fellowship from the Swiss National Science Foundation (Grant P2EZP2 191885). F.d.J. acknowledges funding from the Spanish MCI/AEI/FEDER (Grant PID2021-128760NB-I00). M.G.V. acknowledges the Spanish Ministerio de Ciencia e Innovación (Grant PID2019-109905GB-C21) and Deutsche Forschungsgemeinschaft [Grant GA 3314/1-1-FOR 5249 (QUAST)]. P.A. acknowledges support from the EPiQS program of the Gordon and Betty Moore Foundation (Grant GBMF9452).

■ REFERENCES

(1) Hulliger, F. Crystal chemistry of the chalcogenides and pnictides of the transition elements. *Struct. Bonding (Berlin)* **1968**, *4*, 83−229.

(2) Wehmeier, F. H.; Keve, E. T.; Abrahams, S. C. Preparation, structure, and properties of some chromium selenides. Crystal growth with selenium vapor as a novel transport agent. *Inorg. Chem.* **1970**, *9*, 2125−2131.

(3) Huisman, R.; de Jonge, R.; Haas, C.; Jellinek, F. Trigonal-prismatic coordination in solid compounds of transition metals. *J. Solid State Chem.* **1971**, *3*, 56−66.

(4) Goodenough, J. B. Band model for transition-metal chalcogenides having layer structures with occupied trigonal-bipyramidal sites. *Mater. Res. Bull.* **1968**, *3*, 409−415.

(5) Liang, W. Y.; Cundy, S. L. Electron energy loss studies of the transition metal dichalcogenides. *Philos. Mag.* **1969**, *19*, 1031−1043.

(6) Haas, C. Phase transitions in transition-metal chalcogenides. *Solid State Commun.* **1966**, *4*, 419−421.

(7) Gorkov, L. P., Grüner, G., Eds. Charge density waves in solids. *Modern Problems in Condensed Matter Sciences*; North-Holland: Amsterdam, The Netherlands, 1989; Vol. *25*.

(8) Wang, Z. Z.; Saint-Lager, M. C.; Monceau, P.; Renard, M.; Gressier, P.; Meerschaut, A.; Guemas, L.; Rouxel, J. Charge density wave transport in $(TaSe_4)_2I$. *Solid State Commun.* **1983**, *46*, 325−328.

(9) Coleman, R. V.; Giambattista, B.; Hansma, P. K.; Johnson, A.; McNairy, W.; Slough, C. G. Scanning tunnelling microscopy of charge-density waves in transition metal chalcogenides. *Adv. Phys.* **1988**, *37*, 559−644.
(10) Liu, J.; Wang, H.; Fang, C.; Fu, L.; Qian, X. van der Waals Stacking-Induced Topological Phase Transition in Layered Ternary Transition Metal Chalcogenides. *Nano Lett.* **2017**, *17*, 467−475.
(11) Manzeli, S.; Ovchinnikov, D.; Pasquier, D.; Yazyev, O. V.; Kis, A. 2D transition metal dichalcogenides. *Nat. Rev. Mater.* **2017**, *2*, 17033.
(12) Patra, A.; Rout, C. S. Anisotropic quasi-one-dimensional layered transition-metal trichalcogenides: synthesis, properties and applications. *RSC Adv.* **2020**, *10*, 36413−36438.
(13) Grüner, G. The dynamics of charge-density waves. *Rev. Mod. Phys.* **1988**, *60*, 1129−1181.
(14) Meerschaut, A.; Rouxel, J. Le seleniure $NbSe_3$: Obtention et structure. *J. Less-Common Met.* **1975**, *39*, 197−203.
(15) Hodeau, J. L.; Marezio, M.; Roucau, C.; Ayroles, R.; Meerschaut, A.; Rouxel, J.; Monceau, P. Charge-density waves in $NbSe_3$ at 145K: crystal structures, X-ray and electron diffraction studies. *J. Phys. C: Solid State Phys.* **1978**, *11*, 4117−4134.
(16) Meerschaut, A.; Guemas, L.; Rouxel, J. Structure and properties of the new phase of the pseudo one-dimensional compound TaS_3. *J. Solid State Chem.* **1981**, *36*, 118−123.
(17) Sambongi, T.; Tsutsumi, K.; Shiozaki, Y.; Yamamoto, M.; Yamaya, K.; Abe, Y. Peierls transition in TaS_3. *Solid State Commun.* **1977**, *22*, 729−731.
(18) Roucau, C.; Ayroles, R.; Monceau, P.; Guemas, L.; Meerschaut, A.; Rouxel, J. Electron diffraction and resistivity measurements on the one-dimensional orthorhombic and monoclinic structures of TaS_3. comparison with $NbSe_3$. *Phys. Status Solidi A* **1980**, *62*, 483−493.
(19) Roucau, C.; Ayroles, R.; Monceau, P.; Guemas, L.; Meerschaut, A.; Rouxel, J. Electron diffraction and resistivity measurements on the one-dimensional orthorhombic and monoclinic structures of TaS_3. comparison with $NbSe_3$. *Phys. Status Solidi A* **1980**, *62*, 483−493.
(20) Hasegawa, K.; Maeda, A.; Uchida, S.; Tanaka, S. Non-linear conductivity of monoclinic TaS_3. *Solid State Commun.* **1982**, *44*, 881−883.
(21) Gressier, P.; Meerschaut, A.; Guemas, L.; Rouxel, J.; Monceau, P. Characterization of the new series of quasi one-dimensional compounds$(MX_4)_nY$ (M = Nb, Ta; X = S, Se; Y = Br, I). *J. Solid State Chem.* **1984**, *51*, 141−151.
(22) Gressier, P.; Guemas, L.; Meerschaut, A. Preparation and structure of ditantalum iodide octaselenide, Ta_2ISe_8. *Acta Crystallogr., Sect. B* **1982**, *38*, 2877−2879.
(23) Meerschaut, A.; Palvadeau, P.; Rouxel, J. Preparation et structure cristalline de $I_{0.33}NbSe_4$ ($I_4Nb_{12}Se_{48}$). *J. Solid State Chem.* **1977**, *20*, 21−27.
(24) Zubko, M.; Kusz, J.; Prodan, A.; Šturm, S.; van Midden, H. J. P.; Bennett, J. C.; Dubin, G.; Zupanič, E.; Böhm, H. Structural phase transition and related electronic properties in quasi-one-dimensional $(NbSe_4)_{10/3}I$. *Acta Crystallogr., Sect. B* **2013**, *69*, 229−237.
(25) Philipp, A.; Mayr, W.; Kim, T. W.; Alavi, B.; Maki, M.; Grüner, G. Dynamics of the charge-density-wave mode in $(NbSe_4)_2I$. *Phys. Rev. B* **1989**, *39*, 7536−7544.
(26) Gressier, P.; Guémas, L.; Meerschaut, A. $(NbSe_4)_3I$ low temperature structure. *Mater. Res. Bull.* **1985**, *20*, 539−548.
(27) Wang, Z. Z.; Monceau, P.; Renard, M.; Gressier, P.; Guemas, L.; Meerschaut, A. Charge density transport in a novel halogened transition metal tetrachalcogenide $(NbSe_4)_{3.33}I$. *Solid State Commun.* **1983**, *47*, 439−443.
(28) Fujishita, H.; Sato, M.; Hoshino, S. Incommensurate superlattice reflections in quasi one dimensional conductors, $(MSe_4)_2I$ (M = Ta and Nb). *Solid State Commun.* **1984**, *49*, 313−316.
(29) Fujishita, H.; Sato, M.; Hoshino, S. X-ray diffraction study of the quasi-one-dimensional conductors $(MSe_4)_2I$ (M = Ta and Nb). *J. Phys. C: Solid State Phys.* **1985**, *18*, 1105−1114.
(30) Binnewies, M.; Glaum, R.; Schmidt, M.; Schmidt, P. Chemical Vapor Transport Reactions − A Historical Review. *Z. Anorg. Allg. Chem.* **2013**, *639*, 219−229.
(31) Maki, M.; Kaiser, M.; Zettl, A.; Grüner, G. Charge density wave transport in a novel inorganic chain compound, (TaSe4)2I. *Solid State Commun.* **1983**, *46*, 497−500.
(32) Gooth, J.; Bradlyn, B.; Honnali, S.; Schindler, C.; Kumar, N.; Noky, J.; Qi, Y.; Shekhar, C.; Sun, Y.; Wang, Z.; Bernevig, B. A.; Felser, C. Axionic charge-density wave in the Weyl semimetal $(TaSe_4)_2I$. *Nature* **2019**, *575*, 315−319.
(33) Shi, W.; Wieder, B. J.; Meyerheim, H. L.; Sun, Y.; Zhang, Y.; Li, Y.; Shen, L.; Qi, Y.; Yang, L.; Jena, J.; Werner, P.; Koepernik, K.; Parkin, S.; Chen, Y.; Felser, C.; Bernevig, B. A.; Wang, Z. A charge-density-wave topological semimetal. *Nat. Phys.* **2021**, *17*, 381−387.
(34) Zhang, Y.; Lin, L.-F.; Moreo, A.; Dong, S.; Dagotto, E. First-principles study of the low-temperature charge density wave phase in the quasi-one-dimensional Weyl chiral compound $(TaSe_4)_2I$. *Phys. Rev. B* **2020**, *101*, 174106.
(35) Yi, H.; Huang, Z.; Shi, W.; Min, L.; Wu, R.; Polley, C. M.; Zhang, R.; Zhao, Y.-F.; Zhou, L.-J.; Adell, J.; Gui, X.; Xie, W.; Chan, M. H. W.; Mao, Z.; Wang, Z.; Wu, W.; Chang, C.-Z. Surface charge induced Dirac band splitting in a charge density wave material $(TaSe_4)_2I$. *Phys. Rev. Res.* **2021**, *3*, 013271.
(36) Kim, S.; McKay, R. C.; Bielinski, N.; Zhao, C.; Lin, M.-K.; Hlevyack, J. A.; Guo, X.; Mo, S.-K.; Abbamonte, P.; Chiang, T.-C.; Schleife, A.; Shoemaker, D. P.; Bradlyn, B.; Mahmood, F. Kramers-Weyl fermions in the chiral charge density wave material $(TaSe_4)_2I$. *arXiv* **2021**, DOI: 10.48550/arXiv.2108.10874
(37) Favre-Nicolin, V.; Bos, S.; Lorenzo, J. E.; Hodeau, J.-L.; Berar, J.-F.; Monceau, P.; Currat, R.; Levy, F.; Berger, H. Structural Evidence for Ta-Tetramerization Displacements in the Charge-Density-Wave Compound $(TaSe_4)_2I$ from X-Ray Anomalous Diffraction. *Phys. Rev. Lett.* **2001**, *87*, 015502.
(38) Sinchenko, A. A.; Ballou, R.; Lorenzo, J. E.; Grenet, T.; Monceau, P. Does $(TaSe_4)_2I$ really harbor an axionic charge density wave? *Appl. Phys. Lett.* **2022**, *120*, 063102.
(39) See the Supporting Information.
(40) Sheldrick, G. M. A short history of *SHELX*. *Acta Crystallogr., Sect. A* **2008**, *64*, 112−122.
(41) Sheldrick, G. M. Crystal structure refinement with *SHELXL*. *Acta Crystallogr., Sect. C* **2015**, *71*, 3−8.
(42) Dolomanov, O. V.; Bourhis, L. J.; Gildea, R. J.; Howard, J. A. K.; Puschmann, H. *OLEX2*: a complete structure solution, refinement and analysis program. *J. Appl. Crystallogr.* **2009**, *42*, 339−341.
(43) Toby, B. H.; Von Dreele, R. B. *GSAS-II*: the genesis of a modern open-source all purpose crystallography software package. *J. Appl. Crystallogr.* **2013**, *46*, 544−549.
(44) Kresse, G.; Furthmüller, J. Efficient iterative schemes for ab initio total-energy calculations using a plane-wave basis set. *Phys. Rev. B* **1996**, *54*, 11169−11186.
(45) Kresse, G.; Furthmüller, J. Efficiency of ab-initio total energy calculations for metals and semiconductors using a plane-wave basis set. *Comput. Mater. Sci.* **1996**, *6*, 15−50.
(46) Perdew, J. P.; Burke, K.; Ernzerhof, M. Generalized Gradient Approximation Made Simple. *Phys. Rev. Lett.* **1996**, *77*, 3865−3868.
(47) Tran, F.; Blaha, P. Accurate Band Gaps of Semiconductors and Insulators with a Semilocal Exchange-Correlation Potential. *Phys. Rev. Lett.* **2009**, *102*, 226401.
(48) Blöchl, P. E.; Jepsen, O.; Andersen, O. K. Improved tetrahedron method for Brillouin-zone integrations. *Phys. Rev. B* **1994**, *49*, 16223−16233.
(49) Yaich, H.; Jegaden, J.; Potel, M.; Sergent, M.; Rastogi, A.; Tournier, R. Nouveaux chalcogénures et chalcohalogénures à clusters tétraédriques Nb_4 ou Ta_4. *J. Less-Common Met.* **1984**, *102*, 9−22.
(50) Schmidt, P. J.; Thiele, G. $Nb_2Se_2I_6$: Eine neue Strukturvariante bei Niobchalkogenidhalogeniden mit Kettenstruktur. *Z. Anorg. Allg. Chem.* **1999**, *625*, 1056−1058.

https://doi.org/10.1021/acs.inorgchem.2c03796
Inorg. Chem. 2023, 62, 3067−3074

(51) Gressier, P.; Whangbo, M. H.; Meerschaut, A.; Rouxel, J. Electronic structures of transition-metal tetrachalcogenides $(MSe_4)_nI$ (M = Nb, Ta). *Inorg. Chem.* **1984**, *23*, 1221−1228.

https://doi.org/10.1021/acs.inorgchem.2c03796
Inorg. Chem. 2023, 62, 3067−3074